Available online at www.sciencedirect.com
ScienceDirect
Journal of the European Ceramic Society 29 (2009) 3105–3111
www.elsevier.com/locate/jeurceramsoc

Modelling the tap density of inorganic powders using neural networks

Vincent Moreschi [a,1], Sylvain Lalot [b,2], Christian Courtois [a,*], Anne Leriche [a,3]

[a] Univ Lille Nord de France, F-59000 Lille, France; UVHC, LMP, F-59600 Maubeuge, France
[b] Univ Lille Nord de France, F-59000 Lille, France; UVHC, LME, F-59313 Valenciennes, France

Received 13 February 2009; received in revised form 12 May 2009; accepted 25 May 2009
Available online 7 July 2009

Abstract

In the present study, the tap relative density of five inorganic powders is modelled using neural networks. These powders are similar in shape but have different true density. A large number of mixings are prepared from three classes (coarse, medium, and fine particles) and modelled. The inputs of the neural networks are the 23 weight percentage intervals of the grain size distribution (38–2000 μm). The estimated values are compared to those obtained by factorial plans. It is shown that very accurate results are obtained with a unique relatively small neural network. Finally, the neural network is used to determine the mixing leading to the highest tap relative density.

Keywords: Tap relative density; Inorganic powder; Neural network; Modelling

1. Introduction

Packing of granular matters has long interested specialists of powder technologies and applications.[1,2] When dealing with inorganic matter, the studies mainly focus on the behaviour of the powder during packing. The goal is then to obtain the highest compactness, to reach the highest density. Since the early 1930s a lot of models have been developed to propose the best granular distribution achieving this goal.[3–7] Along with these models, researchers have studied the way powders behave during the successive stages of the compaction process.[8–11] In fact, for a specified granular distribution, the final density strongly depends on the way the particles interact and/or are spatially distributed. Hence, there is no unique value for the density, even for tapped powders.

Nevertheless, it is possible to define an ideal granular distribution, linked to an ideal spatial distribution, leading to the highest density after compaction. This can briefly be described as follows: the voids existing between large particles are occupied by smaller particles; and the voids between these smaller particles are occupied by even more smaller particles; and so on until all space is occupied. This is an ideal situation, and is the basis of a lot of models. Furnas[1,6] founded his model on discrete size distribution, and Andreasen[5] used a continuous particle size distribution. The latter has proposed to use the following equation to compute the granular distribution:

$$\frac{\mathrm{CPFT}}{100} = \left(\frac{D}{D_L}\right)^n$$

where CFPT stands for Cumulative Percent Finer Than, D is the particle size, D_L is the largest particle size, n is the distribution modulus

Andreasen states, that to obtain the highest tap density, "n" should be included in the [0.33, 0.50] interval.

As there is always a smallest particle size D_S, Dinger and Funk[8] have introduced this parameter in the Andreasen model:

$$\frac{\mathrm{CPFT}}{100} = \frac{D^n - D_S^n}{D_L^n - D_S^n}$$

and state that the distribution modulus n should be 0.37 to achieve best packing.

* Corresponding author. Tel.: +33 32 03 27 53 16 69; fax: +33 32 03 27 53 16 76.
E-mail addresses: vincent.moreschi@univ-valenciennes.fr (V. Moreschi), sylvain.lalot@univ-valenciennes.fr (S. Lalot), chrisitian.courtois@univ-valenciennes.fr (C. Courtois), anne.leriche@univ-valenciennes.fr (A. Leriche).
URLs: http://www.univ-valenciennes.fr (V. Moreschi), http://www.univ-valenciennes.fr/LME (S. Lalot), http://www.univ-valenciennes.fr (C. Courtois), http://www.univ-valenciennes.fr (A. Leriche).
[1] Tel.: +33 32 03 27 53 16 60; fax: +33 32 03 27 53 16 76.
[2] Tel.: +33 327 511 973; fax: +33 327 511 961.
[3] Tel.: +33 32 03 27 53 16 66; fax: +33 32 03 27 53 16 76.

0955-2219/$ – see front matter © 2009 Elsevier Ltd. All rights reserved.
doi:10.1016/j.jeurceramsoc.2009.05.029

Table 1
Tap specific gravities.

Powder #1	Powder #2	Powder #3	Powder #4	Powder #5
0.6683	0.6154	0.5936	0.5604	0.5797

It has been found that these models do not lead to the maximum experimental values. The morphology of the particles is mainly invoked, e.g. Ref. [10]. Then, authors try to model the apparent density using new characteristics such as the mean particle size, the width of the size distribution, the true density, the shape and shape factor.[12–15] More recently, new tools have been used such as factorial design[16] and neural networks.[17,18] In Ref. [16], it is experimentally shown that, starting from three classes of powder (coarse, medium, and fine), the highest apparent density is obtained using a mix of about 50% of coarse particles and about 50% of fine particles.

Artificial neural networks (ANN) are more and more used in various fields of powder technologies (e.g. Refs. [19–24] to name a few). In Ref. [17], the author studies the possibility to model the density of two powders after compaction and sintering, but does not conclude positively for both; only one being correctly modelled. In Ref. [18], the authors obtained good results but studied a mix of three classes having a very narrow size distribution.

In the present study, the tap density of five inorganic powders is modelled using neural networks; for confidentiality reasons, the powders will be named Powder #1 to Powder #5. Due to the fact that the true densities of the powders are not equal, the tap relative density is modelled. The latter is defined as the ratio of the tap density to the true density. Hence, a perfectly tapped powder would get a value of unity for its tap relative density. The first part is dedicated to the presentation of the preparation and to the characterization of the powders. The following part deals with the use of ANN. It presents the results, including a comparison with the results coming from the use of the factorial design, and the application to mixing optimization.

2. Methods and materials

As already mentioned, the experimental densities (apparent densities) are lower than the optimal density. They strongly depend on the way the powders are prepared and then tapped. So, this section is dedicated to the presentation of the method used in this study.

In a first step, the powders are obtained by grinding. So, they all have a similar morphology (angular). They are all quite light, having quite close tap relative density, but having different particle size distribution.

Table 3
d_{10}, d_{50} and d_{90} equivalent diameters.

	d_{10} (μm)	d_{50} (μm)	d_{90} (μm)
1	127	688	1279
2	148	567	1003
3	372	760	1321
4	321	671	1106
5	302	647	1057

2.1. Characterization techniques

2.1.1. The tap density

To be able to accurately compare results between laboratories and powders, standard procedures have been defined such as USP and ASTM methods. In the present study, the ASTM standard B527 has been used.

To be able to compute the tap relative density, the true density is needed. The latter is measured using helium pycnometry (Ultrapycnometer 1000, Quantachrome). Table 1 gives the tap relative density for the five powders.

2.1.2. The grain size distribution

The grain size distribution of powders is measured by means of laser diffraction. The mathematical model is the Fraunhofer model. In this model, the particles are assimilated to spheres that are completely opaque. In the present study a MasterSizer 2000® (Malvern) has been used. The particles have been dispersed in an air flow using a 0.5 bar pressure (dry test). With this equipment, it is possible to choose the number of the distribution intervals from 2 up to 100. For this study, to get the highest possible accuracy without increasing too much the number of data, it has been chosen to use 23 intervals as defined in Table 2.

It is also possible to get the three following equivalent diameters: d_{10}, d_{50} and d_{90}; where d_{xx} is defined as the diameter where the particles occupying xx vol.% of the powder have a smaller equivalent diameter. Table 3 gives the value for the five powders. Fig. 1 shows the particle size distributions.

2.1.3. SEM observation

A Hitachi S-3500N scanning electron microscope (SEM) has been used to observe the powders. The acceleration voltage has been fixed to 20 kV; the samples have been disposed on a graphite paper and then covered by a thin layer of gold. Fig. 2 shows typical examples of particles for the three grain size classes.

2.2. Powder classification

To split the powders in three, a mechanical sieving has been done (in the dry phase). This has been carried out according to the

Table 2
The 23 intervals of the particle size distribution.

μm	38–45	45–53	53–63	63–75	75–90	90–106	106–125
125–150	150–180	180–212	212–250	250–300	300–355	355–425	425–500
500–600	600–710	710–850	850–1000	1000–1180	1180–1400	1400–1700	1700–2000

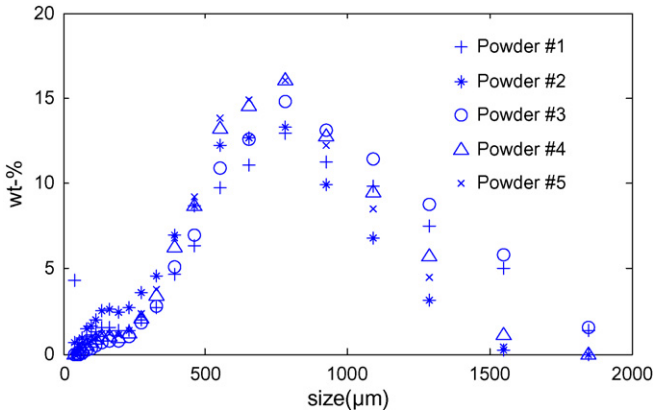

Fig. 1. Particle size distribution for all powders used in this study.

ASTM E11 standard during 15 min. The first size range, hereafter referred to as "coarse particles", is the [1000 μm, 2000 μm] interval. The second size range, hereafter referred to as "medium particles", is the [250 μm, 1000 μm] interval. The last size range, hereafter referred to as "fine particles", is the [38 μm, 250 μm]. Then, apart from the raw powder, 17 mixing have been prepared, as described in Table 4.

Each mixing sample, weighing 100 g, is homogenized in a Turbula®[14] type blender–mixer for 3 min. SEM observations and laser diffraction measurements show no modification of the particles in terms of particle size distribution and particle shape. It can be concluded that the blending/mixing process do not alter the characteristics of the powders.

3. Artificial neural networks (ANN)

3.1. Principles

It is now well known that ANN can be used to represent non-linear systems. For example, they are used in thermal engineering,[25–27] chemical engineering,[28–30] and in system identification[31–33]; see Ref. [34] for an introduction to ANN.

In this study, ANN are used to model the tap relative density, taking the 23 intervals of the weight% distribution as inputs (see Table 2). In fact, as usually done, the inputs and the outputs are pre-/post-processed to get a 0 mean value and a unity standard deviation during the neural process. This locates the computed values in the most sensitive part of all transfer functions (linear and non-linear).

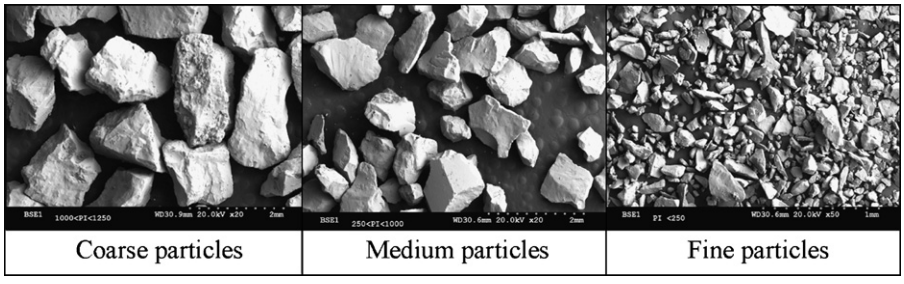

Fig. 2. Examples of SEM observations.

Table 4
Mixing definitions.

Mixing #	Used for test (Powder #)	Coarse particles (wt%)	Medium particles (wt%)	Fine particles (wt%)	Tap relative density				
					Powder #1	Powder #2	Powder #3	Powder #4	Powder #5
1		50	0	50	0.75	0.64	0.66	0.64	0.67
2	3	0	0	100	0.60	0.53	0.59	0.53	0.59
3		0	100	0	0.61	0.55	0.55	0.52	0.56
4		100	0	0	0.57	0.55	0.54	0.52	0.56
5	3	16.67	16.67	66.67	0.70	0.58	0.63	0.58	0.63
6	2	50	50	0	0.61	0.56	0.56	0.55	0.57
7		16.67	66.67	16.67	0.67	0.58	0.59	0.56	0.59
8		0	50	50	0.72	0.60	0.61	0.58	0.63
9		66.67	16.67	16.67	0.68	0.56	0.61	0.58	0.61
10	1 and 2	33.33	33.33	33.33	0.73	0.62	0.61	0.60	0.65
11		32	21	47	0.74	0.64	0.66	0.62	0.67
12	5	26	20	54	0.73	0.60	0.63	0.60	0.65
13		83	9	8	0.62	0.58	0.58	0.56	0.59
14	5	72	0	28	0.70	0.62	0.66	0.58	0.63
15	4	26	0	74	0.69	0.58	0.63	0.58	0.63
16	1	0	78	22	0.69	0.56	0.58	0.56	0.61
17		25	75	0	0.62	0.56	0.56	0.55	0.57
18	4	raw powder			0.67	0.62	0.59	0.56	0.61

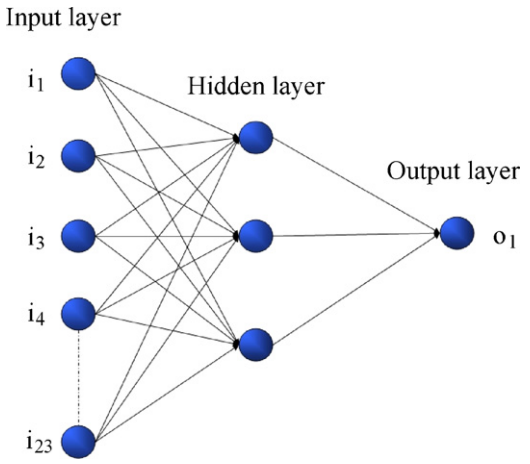

Fig. 3. Schematic of a standard feed forward neural network having 23 inputs and one output.

Concerning the number of neurons on the hidden layer, it is important to note that only 90 sets of inputs are available (18 mixing for each of the five powders). Hence, considering the 23 inputs and the bias for each neuron, three neurons is the maximum. This corresponds to 23×3 connection weights between the inputs and the hidden layer, three connection weights between the biases and the hidden neurons, three connection weights between the hidden neurons and the output neuron, and one connection weight between the output neuron and its bias, which makes a total of 76 connection weights (see Fig. 3 for a simplified schematic of a neural network). Adding a fourth hidden neuron would add 25 connection weights, leading to a number of parameters higher than the number of equations. In this case, a perfect fit could be achieved between estimated data and actual data included in the training set, but a very poor fit is generally observed for data included in the test set. This fact is known as over fitting. On the contrary, using too few parameters leads to very bad results, either in the training phase, or in the test phase.

Within the hidden layer the neurons do not necessarily get the same transfer function. So, the hidden layer can be divided into two or more sublayers, each of them using a specific transfer function. It has to be noted that in the case of the linear transfer function, a unique neuron is sufficient in the corresponding sublayer.

The connection weights are determined using a standard optimization procedure known as the training phase. The latter is carried out using a part of the whole database (training dataset). The remaining data are used for testing. In the present study, to keep a satisfactory number of data for the test phase, it has been chosen to use 90% of the whole dataset for training; hence 10% of the database is used for testing. These 10% are chosen so that all powders have 10% left for tests; but within a powder, these 10% are randomly extracted; see Table 4.

This optimization has to be repeated for all neural network architectures tested. The latter are defined as sets of number of neurons and transfer functions. Finally the optimal structure is selected based on the highest efficiency obtained.

It is possible to use various criteria to measure this efficiency. It can be the correlation coefficient(s) between actual outputs and the estimated outputs using the whole database and/or only the test dataset; it can be a combination of the correlation coefficient(s), the mean average error(s), and the standard deviation(s). It has been chosen here to find a good compromise between the correlation coefficient (training dataset), the maximum absolute error (test dataset), and the mean error (test dataset).

In the present study, the Neural Network Matlab® toolbox has been used. Hence further details can be found in the user's manual.[35]

3.2. Application

A large number of architectures have been tested. Table 5 shows the most relevant results.

In Table 5:

- linear corresponds to: $y = x$;
- non-linear 1 corresponds to: $y = 1/(1 + \exp(-x))$;
- non-linear 2 corresponds to: $y = 2/(1 + \exp(-2x)) - 1$.

The fully linear architecture leads to a correlation coefficient of 0.742, a maximum absolute error of 30.953% and a mean error of 1.309%.

It can be concluded that the link between the particle size distribution and the tap relative density is non-linear. It can be seen that overtraining occurs for test numbers 1 and 2: the correlation coefficient are quite high while the maximum absolute error is also high. On the other hand, the fifth architecture is not well adapted as the correlation coefficient is a little bit lower than the other values, while the errors are higher than the errors for the other tests.

Eventually, test number 3 shows the best compromise. The final architecture is represented in a compact way in Fig. 4.

Table 5
Most relevant results.

Test #	Transfer function of the output neuron	Number of neurons on the first hidden sublayer	Transfer function used in the first hidden sublayer	Number of neurons on the second hidden sublayer	Transfer function used in the second hidden sublayer	Correlation coefficient	Maximum absolute error (%)	Mean error (%)
1	Linear	2	Non-linear 1	1	Linear	0.976	8.370	0.927
2	Linear	2	Non-linear 1	1	Non-linear 1	0.975	6.109	−0.583
3	**Linear**	**2**	**Non-linear 2**	**1**	**Linear**	**0.975**	**4.733**	**−0.086**
4	Linear	2	Non-linear 2	1	Non-linear 2	0.972	6.490	0.327
5	Linear	2	Non-linear 2	1	Non-linear 1	0.973	5.976	−1.284

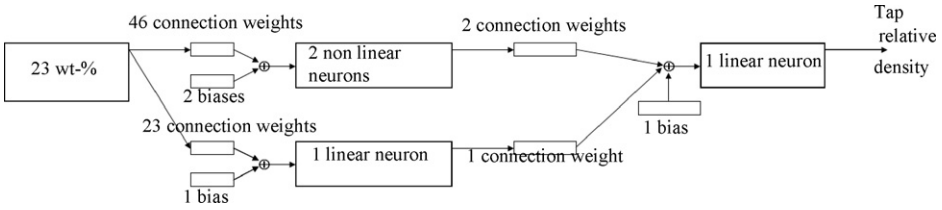

Fig. 4. Compact representation of the selected architecture.

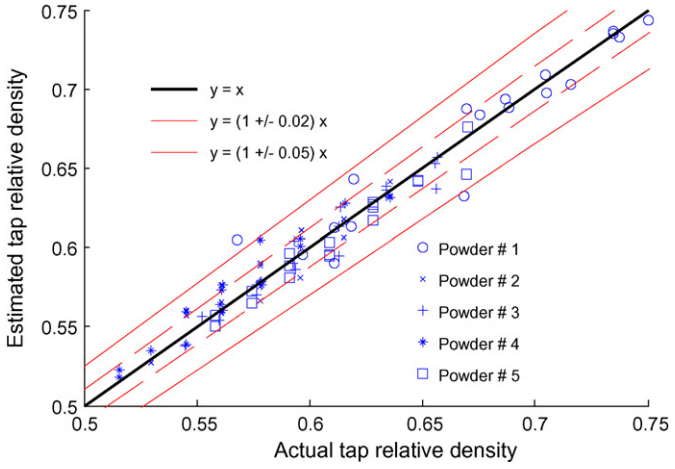

Fig. 5. Overview of all the results obtained by the selected architecture.

3.3. Results

It can be seen (Fig. 2) that the particles are far from being spherical but similar in shape, so that an analytical model for packing would be difficult to determine. It is important to note that this is true for all the powders. Thus, the results are not comparable to those presented in Ref. [36] for perfectly spherical particles.

By using the selected architecture, it is possible to estimate the tap relative density for all samples and to compare these values to the actual values. Fig. 5 shows an overview of the results.

As can be seen, just a very few estimated values are more than 5% away from the actual values. The accuracy of the results can also be estimated by correlation coefficients that are computed for each powder. These are compared (Table 6) to the values obtained when using factorial design that are presented in Ref. [16]. In the latter case, a model is obtained for each powder.

Table 6
Comparison of factorial plans and neural networks accuracy.

Correlation coefficient	Factorial plans	Neural networks
Powder #1	0.94	0.9570
Powder #2	0.70	0.9539
Powder #3	0.87	0.9762
Powder #4	0.73	0.9672
Powder #5	0.81	0.9783

A model developed for only one sand mix leads to similar correlation coefficients.[37]

On one hand, it can be concluded that a specialized tool (one per powder) can be less accurate than a global tool. This is easily explained by the fact that factorial designs lead to linear representations, and that the optimization phase of the neural network has clearly shown that the relation is non-linear. This non-linearity leads to complex shapes for the iso-values (Fig. 6) of the tap density, which is not the case for more standard products as shown in Fig. 5 of Ref. [38].

On the other hand, it can be concluded, as there are no large differences between all correlation coefficients, that there is no "exotic" powder. All of them can accurately be modelled using a unique neural network.

3.4. Mixing optimization

Once the neural network is chosen, it is possible to use it to compute the tap relative density for any weight% distribution, as long as the latter corresponds to a mixing of the three classes (see Table 4). This can be used to determine the mixing that leads to the highest tap relative density. This is similar to what is presented in Ref. [39]. To do so, 66 mixings have been created and used to feed the network. The results are given in Fig. 6.

It can be observed that two powders (#1 and #3) have their maximum located on the lower line (at about the same point), and that the three others have their maximum located in the lower left corner (Fig. 6). This result is surely connected to the fact that these two powders present the highest values of weight percentage for the large particles (Fig. 1). Note that the exact proportions are not given due to confidentiality reasons.

It can also be seen that the mixing leading to the maximum tap relative density is not just a blend of coarse and fine particles as found when using the factorial plans.

In four cases, the maximum tap relative density is about 15% higher than the tap relative density of the raw powder; in the last case, the increase is about 6.5%. In Ref. [37], the optimization process leads to an increase of about 13% between the worst combination (among 54 combinations) and the optimal combination. The highest tap relative density obtained is about 0.75. Although it is less than the 85% which can be theoretically achieved,[36] it has to be noted that the latter case is only possible when considering spherical particles; which is far from the case in the present study (Fig. 2).

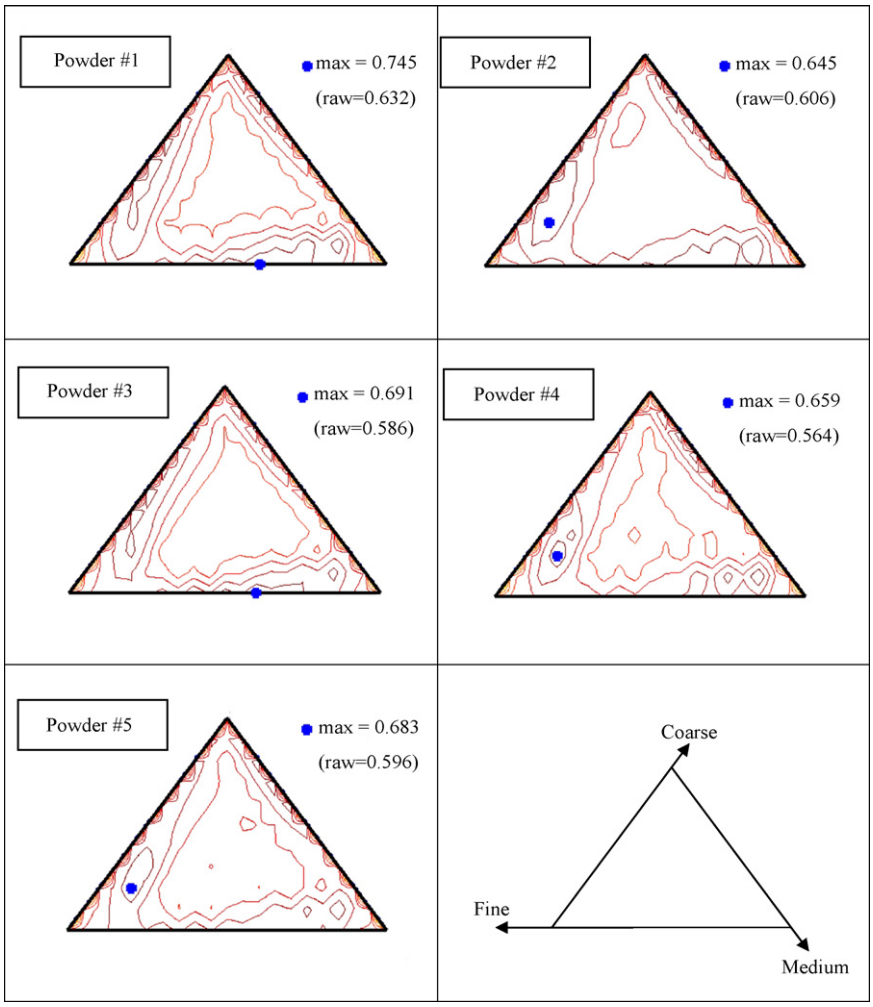

Fig. 6. Prediction of the maximal tap relative density.

4. Conclusions

It has been shown that a neural network can accurately model the tap relative density of powders. An important finding is that it has been possible to find a unique model for five powders. This is possible using the full particle size distribution (23 classes), and a combination of linear and non-linear transfer functions. Nevertheless, it has to be reminded that a random combination of those 23 classes would have surely led to wrong results, as the training database just contain a mixing of pre-defined sieved distributions (coarse, medium, and fine).

Future works will address the study of more powders, surely leading to a more complex model. In particular, it will be checked if it is necessary to have similar shapes (as it is the case in the present study), to be able to model a large number of powders.

References

1. Furnas, C. C., Relations between specific volume, voids and size composition in systems of broken solids of mixed sizes, U.S Bureau of Mines Report of Investigation, No. 2894, 1928.
2. Dodds, J. A., The structure of random packings formed by spheres with a mixture of sizes. In *The Physics of Granular Media*, ed. D. Bideau and J. A. Dodds. Pub. Nova Science, NY, 1991, ISBN 1-56072-034-4, June.
3. German, R. M., *Particle Packing Characteristics*. Metal Powder Industries Federation, Princeton, NJ, 1989.
4. Grays, W. A., *The Packing of Solid Particles*. Chapman & Hall, London, 1968.
5. Andreasen, A. H. Mn and Andersen, J., Relation between gain size and interstitial space in products of unconsolided granules. *Kolloid-Z.*, 1929, **50**, 217–228.
6. Furnas, C. C., Grading aggragates. I. Mathematical relations for beds of broken solids of maximum density. *Ind. Eng. Chem.*, 1931, **23**, 1052–1058.
7. Westman, A. E. R., The packing of particles: empirical equations for intermediate diameter ratios. *J. Am. Ceram. Soc.*, 1936, **19**, 127–129.
8. Dinger, D. R. and Funk, J. E., Particle packing II, review of packing of polydisperse particle system. *Interceram*, 1992, **41**, 95–97.
9. Liu, S. and Ha, Z., Prediction of random packing limit for multimodal particle mixtures. *Powder Technol.*, 2002, **126**, 283–296.
10. Zheng, J., Johnson, O. F. and Reed, J. S., Improved equation of the continuous particle size distribution for dense packing. *J. Am. Ceram. Soc.*, 1990, **73**(5), 1392–1398.
11. Konakawa, Y. and Ishizaki, K., The particle size distribution for the highest relative density in a compacted body. *Powder Technol.*, 1990, **63**, 241–246.
12. Silva, A. P., Segadaes, A. M. and Devezas, T. C., Optimization of the packing density of alumina powder distributions using statistical techniques. *Ceramica*, 2004, **50**.
13. Dodds, J. A., The relation between the structure of packings of particles and their properties, Physics of finely divided matter. *Proc. Phys.*, 1988, **5**.

14. Suzuki, M., Sato, H., Hasegawa, M. and Hirota, M., Effect of size distribution on tapping of fine powder. *Powder Technol.*, 2001, **118**, 53–57.
15. Zu, R. P. and Yu, A. B., Evaluation of the packing characteristics of monosized non-spherical particles. *Powder Technol.*, 1996, **88**, 71–79.
16. Moreschi, V., PhD Thesis, University of Valenciennes and Hainaut Cambresis, 2008, France.
17. Guerain, V., Prédiction et compréhension de la densification des poudres commerciales d'alumine et de fer grâce à une approche par réseau de neurones artificiels. Ph.D. Thesis. Science des Matériaux, Lausanne, EPFL, 2004.
18. Sutcu, M. and Akkurt, S., ANN model for prediction of powder packing. *J. Eur. Ceram. Soc.*, 2007, **27**, 641–644.
19. Laosiritaworn, W., Khamman, O., Ananta, S., Yimnirun, R. and Laosiritaworn, Y., Artificial neural network modelling of ceramics powder preparation: application to $NiNb_2O_6$. *Ceram. Int.*, 2008, **34**(May (4)), 809–812.
20. Ohdar, R. K. and Pasha, S., Prediction of the process parameters of metal powder perform forging using artificial neural network (ANN). *J. Mater. Process. Technol.*, 2003, **132**(1–3), 227–234.
21. Dihoru, L. V., Smith, L. N. and German, R. M., Experimental analysis and neural network modelling of the rheological behaviour of powder injection moulding feedstocks formed with bimodal powder mixtures. *Powder Metall.*, 2000, **43**, 31–36.
22. Karatas, C., Sözen, A., Arcaklioglu, E. and Erguney, S., Experimental and theoretical investigations of mouldability for feedstocks used in powder injection moulding. *Model. Simul. Eng.*, 2007(2), Article #2.
23. Balasubramanian, M., Paglicawan, M. A., Zhang, Z.-. X., Lee, S. H., Xin, Z.-X. and Kim, J. K., Prediction and optimization of mechanical properties of polypropylene/waste tire powder blends using a hybrid artificial neural network-genetic algorithm (GA-ANN). *J. Thermoplast. Compos. Mater.*, 2008, **21**(1), 51–69.
24. Dihoru, L. V., Smith, L. N., Orban, R. and German, R. M., Experimental analysis and neural network modelling of the stability of powder injection molding feedstocks. *Mater. Manuf. Process.*, 2000, **15**(3), 419–438.
25. Lecoeuche, S., Lalot, S. and Desmet, B., Modelling a non-stationary single tube heat exchanger using multiple coupled local neural networks. *Int. Commun. Heat Mass Transfer*, 2005, **32**(7), 913–922.
26. Kalogirou, S., Lalot, S., Florides, G. and Desmet, B., Development of a neural based fault diagnostic system for solar thermal applications. *Solar Energy*, 2008, **82**, 164–172.
27. Lalot, S., Artificial neural networks in solar thermal energy systems. In *Artificial Intelligence in Energy and Renewable Energy Systems*, ed. S. Kalogirou. Nova Science Publishers, Hauppauge, NY, 2006 [Chapter 3].
28. Keller, R. E., Kouzes, R. T. and Kangas, L. J., Neural network applications in an environmental and molecular sciences laboratory. In *World Congress on Neural Networks*, 1993.
29. Sato, A., Sha, Z. and Palosaari, S., Neural networks for chemical engineering unit operations. *Chem. Eng. Technol.*, 1999, **22**(9), 732–739.
30. Fernandes, F. A. N. and Lona, L. M. F., Neural network applications in polymerization processes. *Braz. J. Chem. Eng.*, 2005, **22**(3).
31. Pham, D. T. and Oh, S. J., Identification of plant inverse dynamics using neural networks. *Artif. Intell. Eng.*, 1999, **13**(3), 309–320.
32. Sjöberg, J., Non linear system identification with neural networks. Ph.D. Thesis, Department of Electrical Engineering, Linköping University, Sweden, 1996.
33. Norgaard, M., Ravn, O., Poulsen, N. K. and Hansen, L. K., *Neural Networks for Modeling and Control of Dynamic Systems*. Springer-Verlag, London, 2000.
34. Haykin, S., *Neural Networks—A Comprehensive Foundation* (*2nd ed.*). Prentice Hall, Upper Saddle River, NJ, 1999.
35. Demuth, H., Beale, M. and Hagan, M., *Neural Network Toolbox 6 User's Guide*. The Mathworks Inc., Natick, MA, 2009.
36. Sobolev, K. and Amirjanov, A., The simulation of particulate packing using a particle suspension model. *Adv. Powder Technol.*, 2007, **18**(3), 261–271.
37. Muthukumar, M., Mohan, D. and Radjendran, M., Optimization of mix proportions of mineral aggregates using Box Behnken design of experiments. *Cement Concrete Compos.*, 2003, **25**, 751–758.
38. Wong, H. H. C. and Kwan, A. K. H., Packing density: a key concept for mix design of high performance concrete, available in 2009 at http://www.hkpc.org/hkiemat/mastec05_program_notes/Prof.%20Albert%20KWAN.pdf.
39. Silva, A. P., Segadaes, A. M. and Devezas, T. C., Aplicação de métodes estatisticos na otimização da densidade de empacotameto de distribuições de pos de alumina. *Ceramica*, 2004, **50**, 345–354.